Microcell atomic clock using laser current-actuated power modulation with 10^{-12} range stability at 1 day

Carlos-Manuel Rivera-Aguilar^{1,*}, Andrei Mursa¹, Clément Carlé¹, Jean-Michel Friedt¹, Emmanuel Klinger¹, Moustafa Abdel Hafiz¹, Nicolas Passilly¹, and Rodolphe Boudot¹

¹FEMTO-ST, CNRS, Université Marie et Louis Pasteur, SupMicrotech-ENSMM, Besançon, France.

ABSTRACT

We present a coherent-population trapping (CPT) microcell atomic clock using symmetric auto-balanced Ramsey (SABR) spectroscopy. The pulsed SABR sequence is applied through direct current-based power modulation of the vertical-cavity surface-emitting laser, eliminating the need for an external optical shutter and enabling compatibility with fully-integrated clocks. The sequence is controlled by a single FPGA-based digital electronics board. A key aspect of proper clock operation was the implementation of a real-time tracking of the atomic signal detection window. The clock frequency dependence on laser power, microwave power, laser frequency, and timing of the detection window has been measured, obtaining sensitivity coefficients lower than those obtained with Ramsey-CPT spectroscopy. The Allan deviation of the SABR-CPT clock, based on a microfabricated cell with low-permeation glass windows, is 8×10^{-10} at 1 s and averages down in the 10^{-12} range at 1 day. These results might stimulate the development of chip-scale atomic clocks using Ramsey-based sequences, with reduced light-shift sensitivity, and enhanced long-term stability performances.

Introduction

Chip-scale atomic clocks (CSACs) based on coherent population trapping (CPT) have met a remarkable success in navigation, communication, defense and synchronization systems by offering a fractional frequency stability at 1 day in the 10^{-11} range in a low size, weight and power (SWaP) budget¹. These clocks rely on the interaction of a hot alkali vapor, confined in a microfabricated vapor cell in the presence of a pressure of buffer gas², with an optically-carried microwave signal obtained by direct current modulation of a vertical-cavity surface emitting laser (VCSEL). Under null Raman detuning condition, atoms are trapped in a quantum dark state³ for which the atomic vapor transparency is increased, leading to the detection of an atomic resonance, used to stabilize the frequency of the local oscillator (LO) that drives the modulation of the VCSEL.

The fractional frequency stability of CSACs is usually degraded for integration times higher than 100 s by light-shifts. Several approaches have been proposed to mitigate light-shifts in CPT-based CSACs. A widely used technique involves tuning the microwave power set point to cancel at the first order the clock frequency dependence to laser power variations. Nevertheless, this microwave power setpoint is specific to the physics-package, may not exist in cells filled with high buffer gas pressures⁷, and only protects the clock frequency from laser power variations. Other techniques, such as the implementation of advanced algorithms for compensation of the laser current-temperature couple⁸, the tuning of the cell temperature⁹, or the use of interrogation sequences based on power-modulation ^{10–12}, have been proposed.

Ramsey spectroscopy is efficient for light-shift reduction. Ramsey-CPT spectroscopy 13,14 , in which atoms interact with a sequence of optical CPT pulses separated by a free-evolution dark time of length T, was performed first in microfabricated cells in Refs 15,16 . The symmetric auto-balanced Ramsey (SABR) sequence 17 , an extended version of the auto-balanced Ramsey (ABR) spectroscopy technique 18 , was later demonstrated to reduce further the clock frequency dependence to laser power, laser frequency and microwave power in CPT clocks 19 . This approach, combined with the use of a microcell made with low permeation glass substrates 20 , has enabled the demonstration of a microcell CPT clock with fractional frequency stability in the low 10^{-12} range at $1 \, \mathrm{day}^{21}$.

Nevertheless, in the studies mentioned above, the pulsed optical sequence was produced using an external optical shutter, typically an acousto-optic modulator (AOM), which is incompatible with a fully-integrated CSAC. To avoid the use of the AOM, a two-step pulse sequence, applied through driving-current-based power modulation of the VCSEL, was proposed and demonstrated^{22–24}. In these studies, Ramsey-CPT spectroscopy was performed in a cm-scale glass-blown vapor cell, while no stability results were reported. In Ref.²⁵, we demonstrated, using the two-step pulse sequence and direct power modulation through the laser current, real-time closed-loop operation of a Ramsey-CPT microcell atomic clock. In this work, a tenfold reduction of the clock frequency sensitivity to laser power compared to the continuous-wave (CW) case was reported. Also, the

^{*}carlos.rivera@femto-st.fr

clock stability, extracted from a measurement of only 10 hours, reached $1.3 \times 10^{-10} \ \tau^{-1/2}$, with limitations after 2000 s likely due to light-shifts and buffer gas permeation through the cell windows.

In this work, we demonstrate a Cs microcell CPT clock based on the SABR interrogation, which offers advantages over the Ramsey-CPT one. Unlike previous works where SABR was implemented using external modulation of the laser 17,19,21 , the SABR sequence, generated using an FPGA-based electronics board, is here produced by directly modulating the VCSEL dc current. This eliminates the need for an AOM for application of the SABR sequence and makes the approach compliant with a fully-integrated CSAC. In the present work, atoms in the microcell experience 170- μ s-long optical CPT pulses, separated by a short dark time T_s of 150 μ s or a long dark time T_L of 250 μ s. The atomic signal is typically measured 18 μ s after the beginning of each pulse in a 1 μ s-long averaging window. An original and important step, needed for proper operation of the clock and never reported before, is the implementation of a detection window tracking system, aimed to compensate for the timing jitter of the detection window caused by current step-induced thermal transients of the laser frequency along the sequence. The clock frequency sensitivity coefficients to laser power, but also to microwave power, laser frequency or timing offset of the detection window, are all measured to be reduced in comparison with those obtained in the Ramsey-CPT regime. The frequency stability of the microcell SABR-CPT clock, extracted from a 3-day measurement, is 8×10^{-10} at 1 s and in the 10^{-12} range at 10^5 s.

Methods

Experimental setup

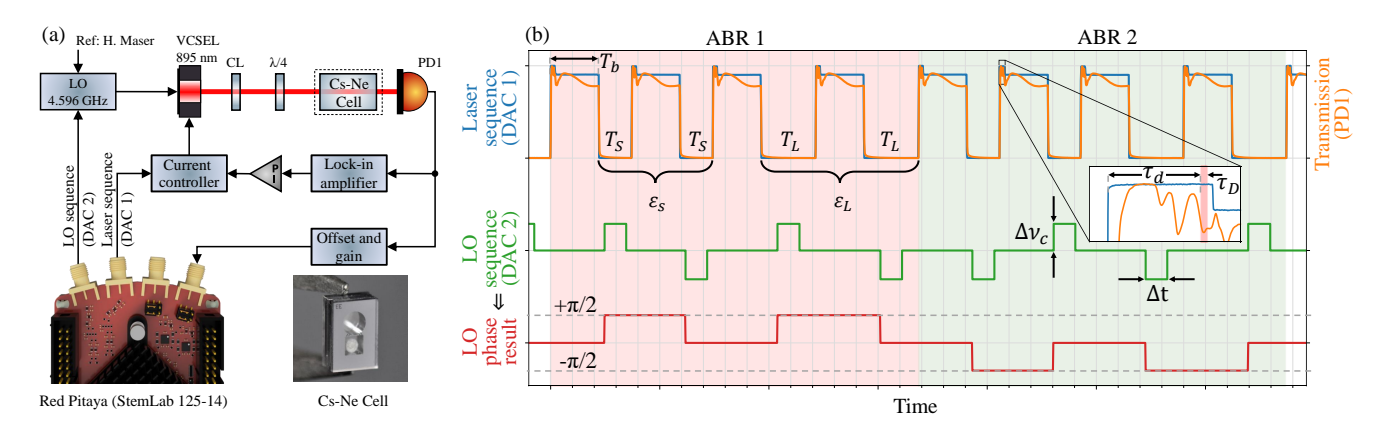


Figure 1. (a) Experimental setup. A hot Cs vapor, confined in a microfabricated vapor cell filled with a buffer gas pressure, interacts with a dual-frequency optical field obtained by direct modulation at 4.596 GHz of the VCSEL current. Atoms are trapped in the CPT dark state using both first-order optical sidebands. The signal at the cell output is used in three servo loops, for laser frequency and LO frequency, as well as light-shift compensation. CL: collimation lens LO: local oscillator. The inset shows a photograph of the Cs-Ne vapor microcell. The experiment is controlled by a single FPGA RedPitaya digital electronics board, shown in the lower-left corner. (b) SABR sequence used for interrogation of the atoms. Instead of interacting continuously with light as in traditional CPT clocks, atoms experience here a sequence of two-step pulses, of total length T_b , separated by free-evolution times (T_S or T_L) in the dark, during which the light is actually turned off by tuning the laser current below the laser threshold current. The pulsed light sequence is then obtained by current-actuated power modulation of the laser. During the "on" portion of the sequence (duration T_b), a detection window is initiated after a delay τ_d and remains open for a time τ_D to enable acquisition of the atomic signal.

The experimental setup, shown in Fig. 1(a), is comparable to the one described in Ref.²⁵. It is a table-top experimental setup intended for proof-of-concept validation. However, the core components are the same than those found in chip-scale atomic clocks and there is a priori no technical limitation for its miniaturization. The laser source is a VCSEL tuned on the Cs D_1 line at 895 nm²⁶. The laser is driven at 4.596 GHz by a commercial microwave synthesizer, noted in this paper as the local oscillator (LO). The latter delivers a microwave power $P_{\mu W}$ of -5.5 dBm (282 μ W) and is referenced to a hydrogen maser for frequency stability and frequency shift measurements. A lens is placed at the output of the laser to collimate the beam. A quarter-wave plate is placed for circularly polarizing the laser beam. The laser light, with a power P_l of 188 μ W, is sent into a physics package at the center of which is inserted a microfabricated Cs vapor cell filled with about 73 Torr (at 0°C) of Ne buffer gas. The cell is stabilized at 82°C. The atom-light interaction takes place in a 2-mm diameter and 1.5-mm long cavity etched in silicon, and filled with alkali vapor through post-sealing laser activation of a pill dispenser^{27,28}. The cell is built with 500- μ m-thick alumino-silicate glass (ASG) windows for reducing buffer gas permeation^{20,21}. A static magnetic field of

250 mG is applied to isolate the clock transition. A single-layer mu-metal magnetic shield protects the atoms from magnetic perturbations. At the output of the cell, the transmitted light is detected by a photodiode that delivers the atomic signal.

Three servo loops are then implemented. The first loop aims to stabilize the laser frequency to the bottom of the absorption profile associated with the $F=3 \rightarrow F'=4$ transition. For this purpose, the laser current is sinusoidally modulated at a frequency of 13.3 kHz while the absorption signal at the photodiode output is demodulated with an external lock-in amplifier for generation of a zero-crossing error signal. This modulation frequency was chosen to avoid overlap with the harmonic components introduced by the square-like two-step sequence sent to the laser, which contains strong higher-order frequency components. When processed with a PI controller, this error signal is exploited to feed-back corrections on the laser dc current. The second servo loop is dedicated to steer the microwave synthesizer output frequency (LO) to the CPT resonance peak. The frequency stability of the clock is assessed by recording the frequency corrections f_c applied to the synthesizer during closed-loop operation. Since the synthesizer is referenced by the maser and the maser stability ($< 10^{-13}$ for $\tau > 1$ s) is significantly better than that of the clock, the measured fluctuations in f_c directly reflect the intrinsic stability of the microcell CPT clock. The third servo loop is devoted to compensate for light-shifts experienced by the atoms during the optical pulses.

SABR-CPT sequence

In Ref.²⁵, Ramsey-CPT spectroscopy was demonstrated in a microcell clock using direct modulation of the laser current. However, Ramsey-CPT spectroscopy suffers from residual sensitivity to light-shifts that can degrade the clock mid- and long-term stability. In the present work, additional efforts were produced to obtain further light-shift mitigation through implementation of the advanced SABR-CPT sequence, still using current-actuated power modulation of the VCSEL.

In Ramsey-CPT spectroscopy, the light-shift created during the light pulses and measured at the end of the Ramsey cycle is inversely proportional to the dark time T^{29} . The essence of the ABR method¹⁸ is then to alternate between two Ramsey sequences with different dark times, a short one, noted T_S , and a long one, noted T_L , resulting in two different light shifts. By comparing the atomic signals obtained for the short (T_S) and long (T_L) cycles, the light shift can be retrieved and corrected in real time.

However, in the case of vapor cell clocks, the pulse repetition rate is comparable to, or even faster than the CPT coherence relaxation rate, preventing the atomic state from being completely reset at each new cycle. In this case, the atoms keep a partial memory of previous interactions, providing a slightly different response depending on the duration of the dark time of the previous sequence. This atomic memory effect leads to a bias in the light-shift estimation and deteriorates the effectiveness of the light-shift reduction method.

In order to cancel this memory effect, the Symmetric ABR (SABR) sequence was proposed¹⁷. The SABR sequence consists of two consecutive ABR sequences (ABR1 and ABR2), the crucial difference being that, in the second sub-sequence (ABR2), the phase of the interrogation signal is inverted. Concretely, the signal is sampled first on the left and then on the right of the fringe during the first sub-sequence (ABR1), while it is sampled on the right and then on the left of the fringe for the second sequence (ABR2). Biases of similar amplitudes but of opposite signs are then obtained in ABR1 and ABR2 sub-sequences, therefore canceling each other out.

The SABR sequence generated in the present work is shown in Fig. 1(b). The sequence consists of two consecutive ABR sequences (ABR1 and ABR2), each composed of four two-step optical pulses of total length T_b . The use of two-step pulses when directly modulating the VCSEL has been shown to effectively reduce the time required for the laser to reach the target atomic optical frequency^{22,25}. The detection window, used for extracting the atomic signal, is opened for a duration $\tau_D = 1~\mu s$, after a short delay τ_d of 18 μs from the beginning of the pulse. For each ABR sequence, the two first Ramsey-CPT patterns use a short dark time T_S while the two next ones use a long dark time T_L . A $\pi/2$ phase jump is applied to the 9.192 GHz interrogation signal during the dark times such that the signal is respectively measured on both sides of the central Ramsey-CPT fringe. As indicated in Fig. 1(b), $\pi/2$ phase jumps are obtained here by generating frequency jumps $\Delta v_c \sim 2.08~kHz$, during a length $\Delta t = 60~\mu s$. Error signals, noted ε_S and ε_L , computed as the difference between the atomic signals measured on both sides of the fringe, are then extracted for the short and long dark time patterns, respectively.

In the second ABR sequence (ABR2), a similar pattern is applied, except that the phase modulation pattern of the 9.192 GHz LO signal is inverted, for obtaining the symmetric interrogation mentioned above. Similarly to previous studies^{17, 19}, two error signals are ultimately generated. The use of these error signals ensures that information is extracted along the sequence at all pulses for both correction signals, reducing the negative impact of aliasing on the short-term stability. The first one, ε_+ = $\varepsilon_S + \varepsilon_L$, is used for stabilization of the LO frequency to the atomic transition. The second one, $\varepsilon_- = \varepsilon_S - \varepsilon_L$, reflects the difference in light shift accumulated during the two dark times and serves as a sensitive discriminator for its compensation.

FPGA implementation

Figure 2 presents a diagram illustrating the implementation of the sequence generation and data processing on the FPGA board. The system is specifically designed to enable precise control of the two servo loops described earlier. It operates at a 125

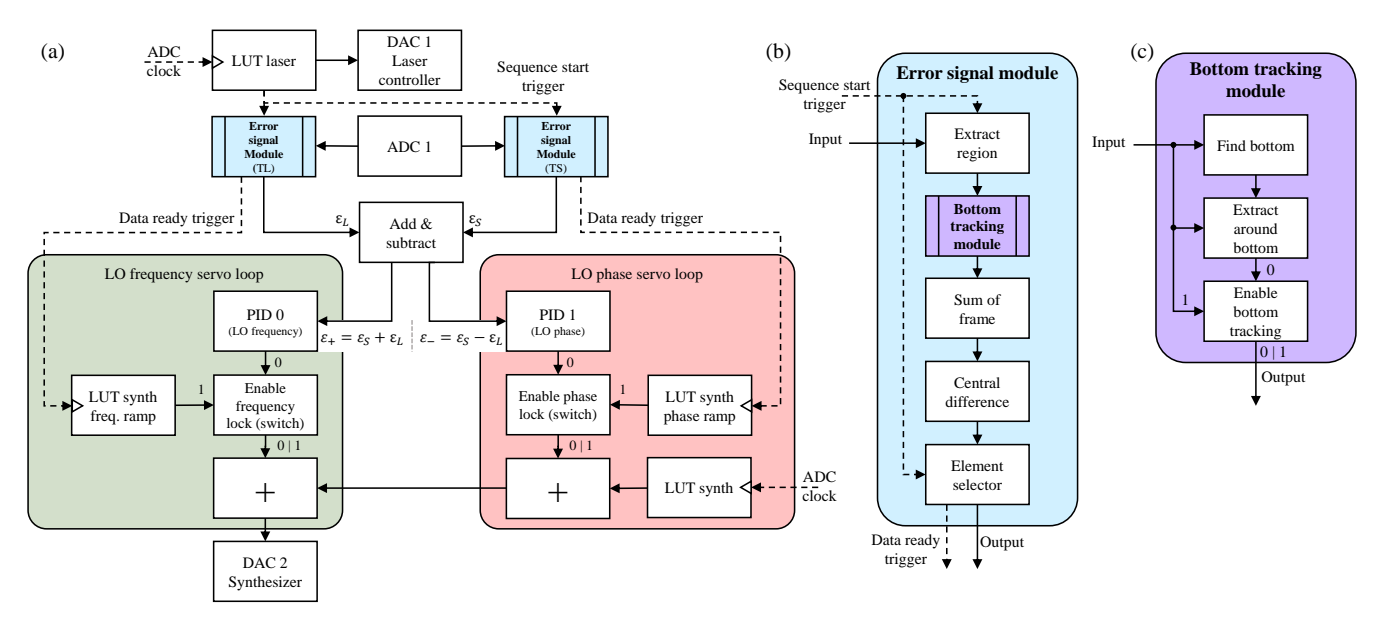


Figure 2. FPGA implementation of the SABR-CPT clock operation.

MHz clock frequency, provided by the analog-to-digital converter (ADC) on the Red Pitaya. The two-step sequence is stored in a Lookup Table (LUT), and its content is sent to a digital-to-analog converter (DAC 1), which is connected to the laser controller. The data acquisition process is synchronized with the start of the sequence generation. As shown in Fig. 2(a), the "sequence start trigger" signal, along with the ADC readings, is fed into the input of the "Error Signal module".

Within the "Error Signal module" (Fig. 2(b)), the first block, "Extract region", isolates a 2 μ s segment at the beginning of each cycle, ensuring that only the portion of the signal corresponding to the correct wavelength is later processed. After the region of interest is extracted, the next stage is the "Bottom tracking module", which returns a 1 μ s segment centered around the bottom of the absorption profile. This step mitigates the effects of jitter and drift in the position of the profile (see details in the next section).

The output of this module is then passed to the "Sum of Frame" block, where it is averaged to produce a single representative point for each cycle. The averaged point is subsequently sent to the "Central Difference" block, which computes the difference between successive points. This step leverages the modulation of the LO (based on the LO LUT content) to extract signals from the left and right sides of the Ramsey fringe. Finally, the "Element Selector" ensures that only differences between consecutive cycles of the same type (T_L or T_S) are used. This is essential due to the interleaved nature of the ABR sequence and the pipelined data processing implemented in the system.

The resulting error signals, ε_S and ε_L , are used to generate error signals ε_+ and ε_- . These error signals are fed into their corresponding PID controllers for either frequency or phase correction. The corrections are applied to the LO sequence stored in "LUT synth", either by adjusting its offset for frequency correction or modifying the amplitude ratio between the ± 2.08 kHz frequency jumps ($\pm \pi/2$ phase jumps) for phase correction. Finally, the modified LO sequence is sent to "DAC 2", which is connected to the modulation input of the microwave synthesizer. Additionally, the system provides the flexibility to apply a ramp instead of frequency or phase corrections, allowing the observation of error signals.

Results

Error signals

Figure 3 shows error signals ε_L (a), ε_S (b), ε_+ (c) and ε_- (d) extracted for a typical interrogation sequence with $T_b = 170~\mu s$, $T_S = 150~\mu s$ and $T_L = 250~\mu s$. Pulses of duration T_b are composed of a first step of length $\tau_1 = 20~\mu s$ and a second step of length $\tau_2 = 150~\mu s$. The error signal ε_S , obtained in cycles with short dark time T_S , is broader and higher in amplitude than the error signal ε_L obtained in cycles with long dark time T_L . The error signal ε_+ benefits from an enhanced amplitude that justifies its use for LO frequency stabilization. The error signal ε_- shows in open-loop configuration a zero-crossing point, image of the light-shift to be compensated.

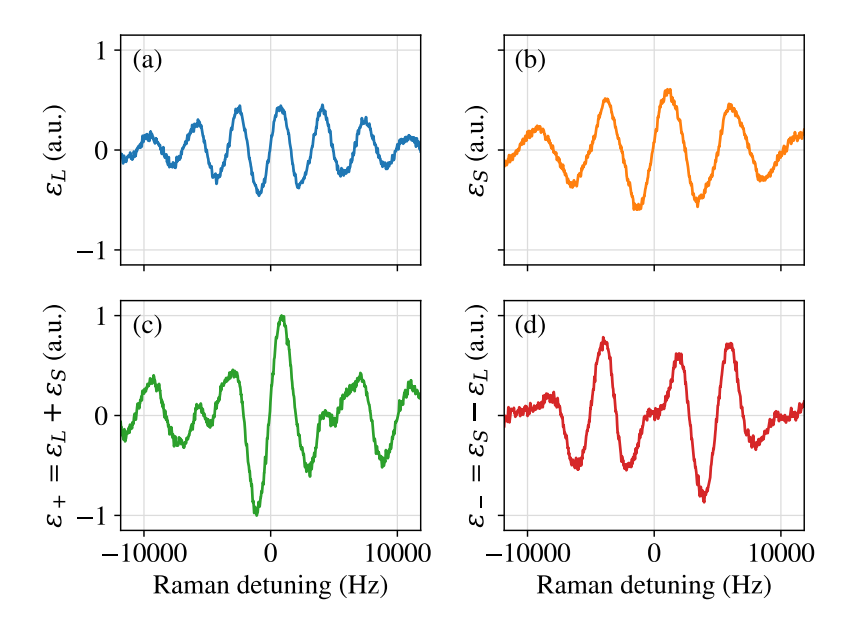


Figure 3. Error signals ε_L (a), ε_S (b), ε_+ (c) and ε_- (d) extracted for a typical interrogation sequence with $T_b = 170 \ \mu s$, $T_S = 150 \ \mu s$ and $T_L = 250 \ \mu s$. ε_+ is used for the LO frequency stabilization while ε_- (d) is exploited for light-shift compensation. The laser power P_l at the cell input is 188 μ W. Each error signal consists of 2046 points, and an 8-sample window moving average was applied to better highlight the signal features.

Detection window tracking

Once the setup implemented and the FPGA programmed, our initial motivation was to measure light-shift coefficients, to assess the efficiency of the SABR-CPT sequence when applied through direct current-based power modulation. However, during initial tests, these measurements, particularly with respect to the laser detuning and the microwave power (which were not investigated in²⁵), proved unreliable and invalid, as the absorption line could move out of the detection window. In the present experiment, the abrupt current pulses induce transient changes of the VCSEL temperature, causing jitter of the laser frequency and consequently shifts of the absorption profile position. Since the atomic signal is extracted from the bottom of this profile, such shifts undermine measurement accuracy.

Figure 4(a) illustrates the jitter of the absorption profile within the detection window, highlighting its temporal fluctuations. The signal was acquired within the FPGA system embedded in the Red Pitaya, directly at the output of the "extract region" block in Fig. 2(b). A total of 36 180 absorption profiles were recorded, non-consecutively, due to data transfer bandwidth limitations, equivalent to 11.57 s of continuous acquisition. These profiles were compiled into a histogram to analyze the probability distribution of their positions over time, revealing fluctuations of approximately ± 40 ns around the position reference.

To observe the temporal evolution of this fluctuation, the position of the absorption profile minimum was extracted using the "find bottom" block in Fig. 2(c) and recorded continuously over a 60-s period, as shown in Fig. 4(b). This confirms that the absorption profile position exhibits significant temporal instability, consistent with observations reported in²³.

We suspected that these fluctuations might affect the clock frequency. A detection window position sweep test was therefore implemented. This study aimed to identify an optimal operating point, and to extract a sensitivity coefficient. Figure 5(a) shows the evolution of the clock frequency versus a timing offset, applied to the 1 μ s-long observation window, relative to the position of the absorption profile bottom at 18.5 μ s from the start of the pulse (as shown in Fig. 5(b)), in both Ramsey-CPT and SABR-CPT modes. In the Ramsey-CPT mode (with $T_b = 170~\mu$ s and $T = 150~\mu$ s), the sensitivity of the clock frequency to the detection window timing is -6.8~mHz/ns, i.e. $7.4 \times 10^{-13}/\text{ns}$ relative to the clock frequency. In the SABR-CPT mode, a stronger dispersion of frequency data points explained by the degradation of the clock short-term stability is observed. Nevertheless, in this mode, we find that the sensitivity of the clock frequency to the detection window timing is -23.35~mHz/ns, i.e. $-2.5 \times 10^{-12}/\text{ns}$ in fractional value. These results emphasized the importance of precisely compensating for the detection window jitter.

To solve this issue, we have implemented on the FPGA a custom real-time absorption line position tracking functionality. This system, depicted in Fig. 2(c), detects the absorption line bottom position within a 1 μ s window and then extracts the data around it. This functionality revolves around the "Extract around bottom" block, which processes a stream of samples (left input as depicted in the diagram) and store them in memory, with each sample assigned an index in an array. Simultaneously,

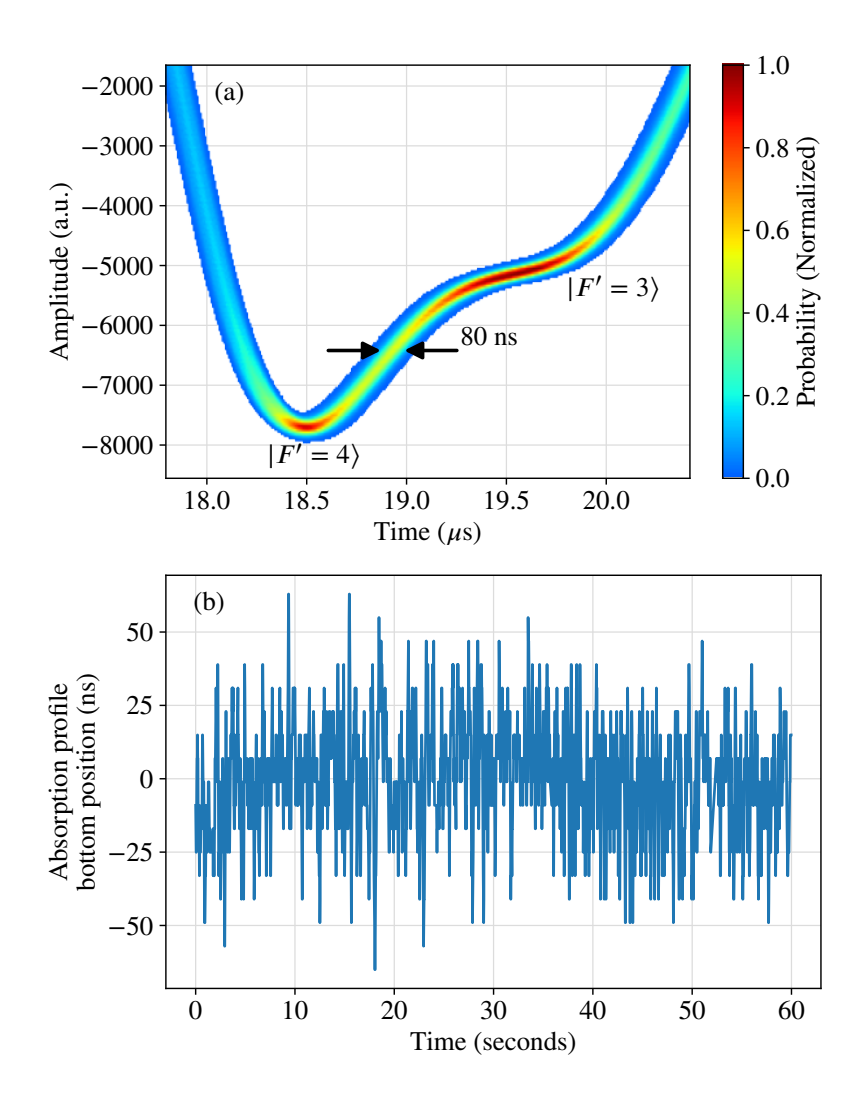


Figure 4. (a) Timing jitter of the absorption profile, and then of the detection window content, induced by current-actuated power modulation of the VCSEL. (b) Temporal trace of the absorption profile bottom position. The amplitude of its fluctuations is about 80 ns.

the block receives an value (input on top in the diagram) that indicates the location of the bottom. Once a 2 μ s window of samples has been collected (providing sufficient data selection), the algorithm calculates the necessary offset to the element indices to ensure that the central element of the produced data corresponds to the detected bottom. Finally, a sequential writing process generates a 1 μ s-long dataset centered around the identified bottom. The implemented method allows the real-time tracking and correction for jitter on every single Ramsey-CPT cycle.

In the SABR-CPT regime, we found that the clock stability could not average down after a few hundreds of seconds before implementation of the detection window tracking. This technique has allowed to significantly mitigate the detrimental impact of the observation window jitter on the clock stability, and has revealed to be a crucial step for performing reliable and repeatable light-shift measurements, as well as demonstrating a clock with enhanced mid- and long-term stability.

Light-shifts

Figure 6(a) shows temporal traces of the clock frequency in Ramsey-CPT (in blue, $T = 150 \mu s$) and SABR-CPT (in orange, $T_S = 150 \mu s$, $T_L = 250 \mu s$) modes. While the clock is running, light-shifts are willingly applied by changing the microwave power that drives the VCSEL. In the Ramsey-CPT case, the clock frequency changes abruptly every time the microwave power is changed. In the SABR-CPT mode, the clock frequency, despite a visible degradation of the signal-to-noise ratio mainly attributed to the increased length of the sequence, remains nearly constant.

Figure 6(b) summarizes the clock frequency shift versus the microwave power in both Ramsey-CPT and SABR-CPT cases. In the Ramsey-CPT case, we measure a sensitivity of $-1.1 \text{ Hz/}\mu\text{W}$. In the SABR-CPT case, we observe a reduction of the

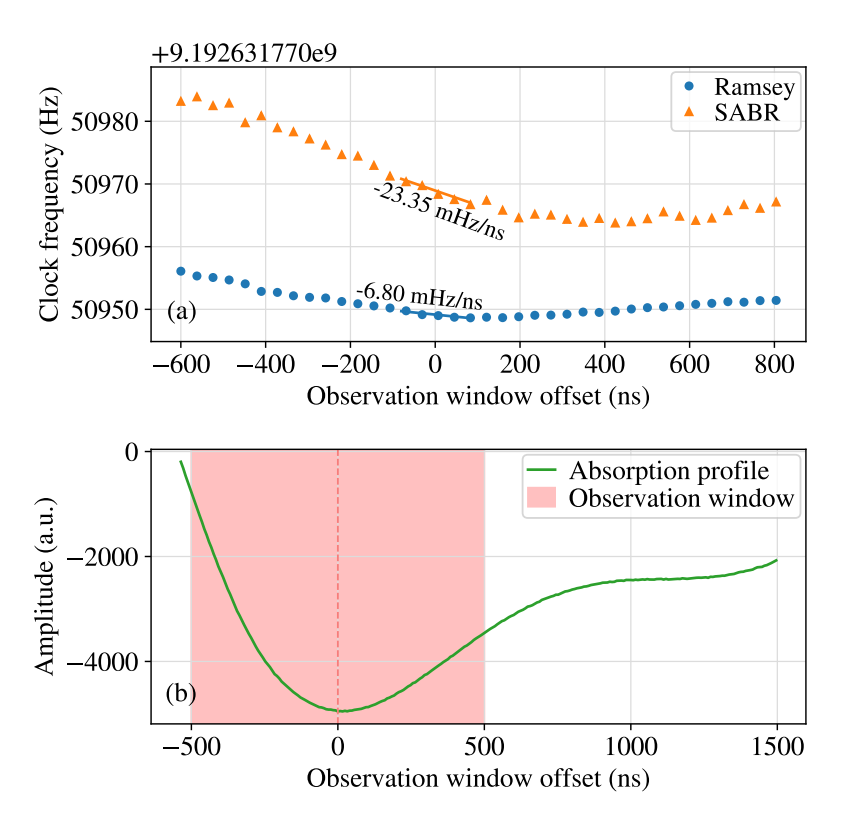


Figure 5. Evolution of the clock frequency with the observation window offset, in both Ramsey-CPT and SABR-CPT modes. A sensitivity of the clock frequency to the observation window offset of -6.8 mHz/ns for Ramsey-CPT and -23.35 mHz/ns for SABR-CPT was found. Parameters are: $P_l = 188 \, \mu \text{W}$ and $P_{\mu W} = -5.5$ dBm. Each point represents the average of 10 repeated measurements per mode. The resulting error bars are smaller than the marker size and not shown.

clock frequency variations by a factor of 27.5, yielding the coefficient of +0.04 Hz/ μ W. This value is close to the one obtained in 19 , where the pulsed sequence was produced with an AOM.

Figures 6(c) and 6(d) report comparable studies as a function of the laser frequency and the total laser power, respectively. Clock frequency sensitivity tests to laser frequency variations were performed by sweeping the laser detuning over a wide range of about \pm 450 MHz. In this range, the clock frequency changes in the Ramsey-CPT case by almost 30 Hz. Also, we notice that a turnover point, around which the sign of the slope is changed and therefore the sensitivity cancelled at the first order, is found close to the null detuning setpoint. In the SABR-CPT case, no turnover point is observed. However, the response is flatter within the whole tested range, yielding an extracted linear coefficient of about 2.5 mHz/MHz, or 2.7×10^{-13} in fractional value. This value is comparable to the one obtained in ¹⁹. Interestingly, we found in this test (Fig. 6(c)), by running the clock in the SABR-CPT regime, that phase corrections applied to the LO to compensate for the light-shift had the same trend as the light-shift curve obtained in the Ramsey-CPT case. This confirms the efficiency of the SABR sequence to tackle residual laser frequency-induced shifts observed in the Ramsey-CPT mode.

For the laser power (Fig. 6(d)), the light-shift trends in both modes exhibit opposite signs (negative for SABR and positive for Ramsey-CPT). The cause of opposite trends, between Ramsey-CPT and SABR-CPT modes, with the laser power, is not clearly understood. In the Ramsey-CPT case, residual light-shifts induced during the light pulses are present and are not compensated. In the ideal SABR-CPT mode, the light-shift should be compensated and the light-shift coefficient should be nulled. Observing a negative light-shift slope in the SABR-CPT regime might result from residual imperfections in the SABR sequence, such as incomplete cancellation of light shifts due to limitations in the dark time values or sequence timing, or residual atomic memory effects not fully suppressed by the symmetric modulation. We note that we have already observed such opposite trends in a high-performance CPT Cs vapor cell clock, described in³⁰ in the Ramsey-CPT mode (positive light-shift slope), and in^{17,31} in the SABR-CPT mode (negative light-shift slope). In the SABR-CPT case, the light-shift slope is found to be reduced at high laser power values. At high power, the fringe signal-to-noise ratio is improved, the light-shift is higher, extracted with better resolution, and then better compensated. We also note that similar trends to the one obtained here in the SABR-CPT mode were obtained in ^{17,31}, with reduced slope at high laser powers. Specifically, in the tested range here,

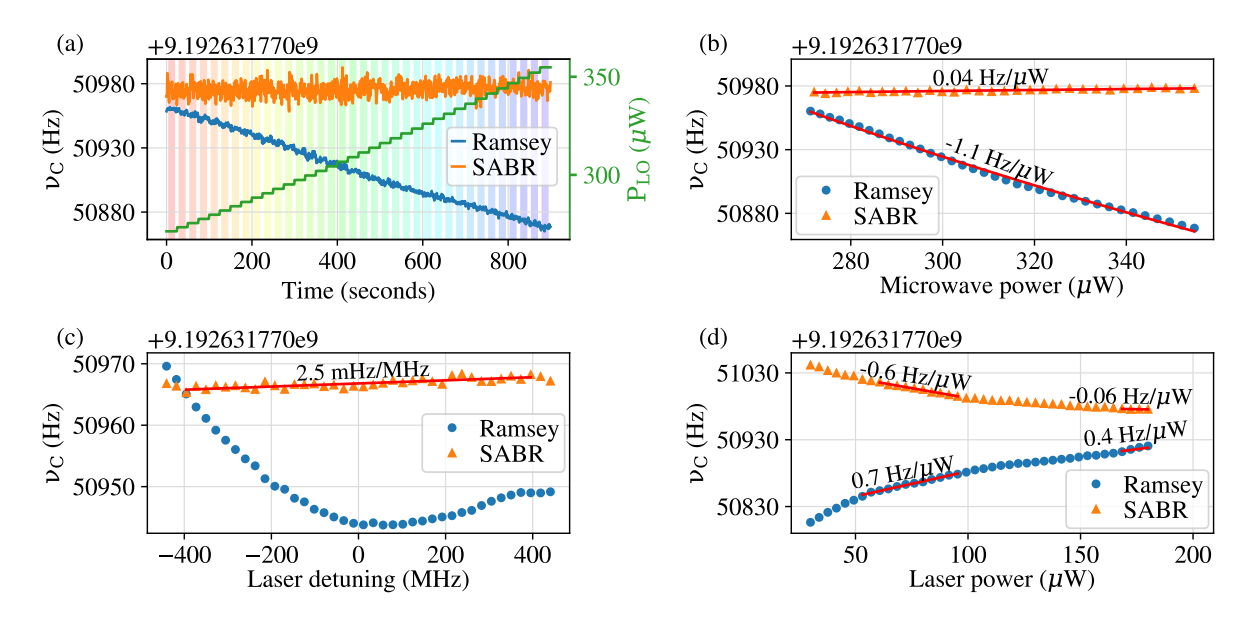


Figure 6. (a) Temporal sequence of the clock frequency. Each step results from the change of the microwave power, inducing a light-shift. Ramsey-CPT and SABR-CPT cases are compared. In the SABR-CPT regime, the clock frequency remains about unchanged despite microwave power jumps. For each microwave power step, the average value of the clock frequency is extracted. Derived from such a sequence, the sub-plot (b) shows the frequency shift of the clock frequency, relative to the unperturbed Cs atom frequency (9.192 631 770 GHz) versus the microwave power. Following a comparable procedure, sub-plots (c) and (d) report the clock frequency shift versus the laser frequency and the laser power, respectively. To change the laser power, a variable neutral density filter was placed before the microfabricated vapor cell (not shown in Fig. 1). If not varied, we use $P_l = 188 \ \mu\text{W}$ and $P_{\mu W} = -5.5 \ \text{dBm}$ (282 μ W). Each point is obtained from 5 averaged light-shift measurements per mode. The associated error bars lie within the marker size.

the light-shift slope in the SABR-CPT mode becomes significantly reduced for $P_l > 160~\mu W$. In the Ramsey-CPT case, the light-shift tends to increase linearly for power values higher than about 120 μW . This suggests that the gain offered by SABR in light-shift mitigation, with respect to the Ramsey-CPT case, might be enhanced at even higher laser power values. With the SABR-CPT sequence, the sensitivity, obtained by fitting the last 4 data points of the curve (corresponding to a laser power range of 12 μW), is measured to be $-0.06~Hz/\mu W$, a factor about 6.7 times lower than the one obtained in the Ramsey-CPT case ($+0.4~Hz/\mu W$) in the same range.

Frequency stability

In the final part of the study, we evaluated the fractional frequency stability of the microcell CPT clock in the SABR-CPT case $(T_S = 150 \ \mu s, T_L = 250 \ \mu s, T_b = 170 \ \mu s, \tau_d = 18 \ \mu s$ and $\tau_D = 1 \ \mu s)$. A 3-day measurement was conducted using our table-top microcell CPT clock prototype. No active laser power or microwave power servo are implemented.

Figure 7 (a) shows the temporal trace of the clock frequency. Figure 7(b) reports the corresponding Allan deviation. The clock fractional frequency stability at 1 s is 8×10^{-10} . This short-term stability is worse than most commercial CSACs but compares favorably to some recently-reported alternative approaches³². Also, it remains sufficiently low to approach the 10^{-11} stability level at 1 hour integration time. We have observed that switching from the Ramsey-CPT to the SABR-CPT sequence (without window tracking) induced a degradation on the short-term stability by a factor of about 4.3 while the activation of the detection window tracking technique could induce an excess degradation by a factor of about 1.9. Nevertheless, the short-term stability of the clock in the SABR-CPT mode could be improved, at least by a factor 2, through some optimizations of the clock parameters and by adopting the laser amplitude noise normalization technique implemented in 17 . Efforts are in progress in this direction but remain out of the main scope of this paper, focused on the mid- and long-term stability. For longer integration times, the clock Allan deviation averages down with a $\tau^{-1/2}$ slope, signature of white frequency noise, to reach the 10^{-12} range at 10^5 s. The stability level at 1 day is comparable to the one obtained in 21 , in which the pulsed sequence was produced with an external AOM. This stability result obtained at 1 day, using laser current-actuated power modulation of the VCSEL and approaching those of best reported CPT-based CSACs 8,21,33 , is then very encouraging to motivate the development of pulsed Ramsey-based CSACs. Before concluding, we note that the clock laser has been now operated in the pulsed regime for more than 2 years. No visible signs of laser or clock signal degradation have been observed so far.

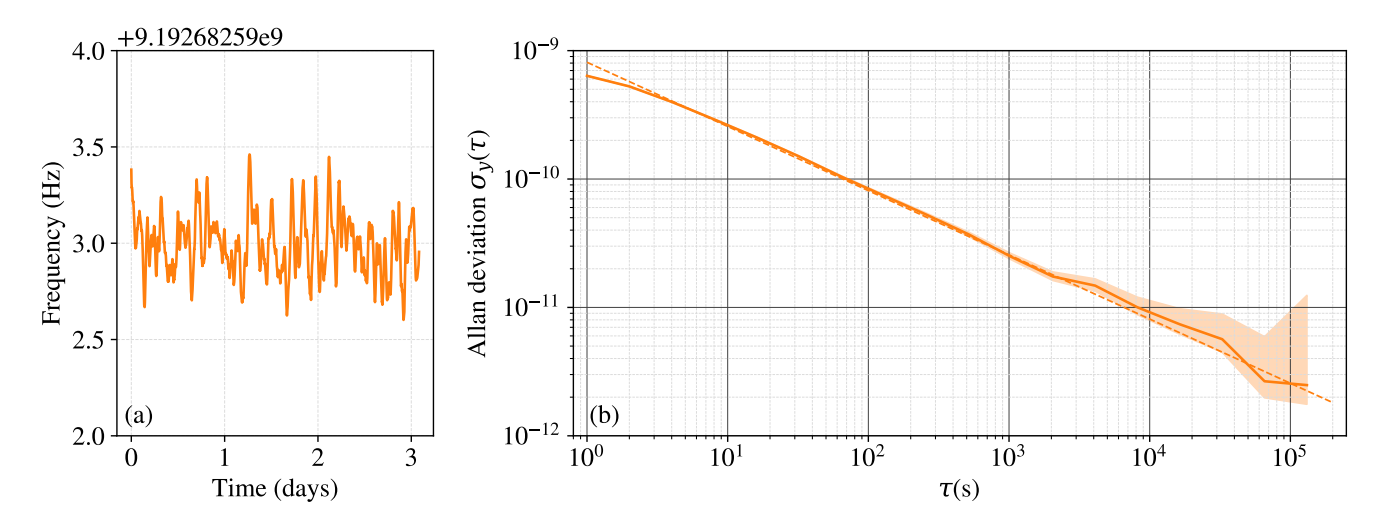


Figure 7. (a) Temporal trace of the clock frequency over 3 days. A 1-hour moving average is applied for illustrative purposes only. (b) Allan deviation of the clock frequency over the 3-day period. The dashed orange line represents the slope of $8 \times 10^{-10} \tau^{-1/2}$

Conclusions

In conclusion, we have demonstrated a CPT-based microcell atomic clock using the pulsed SABR sequence. The SABR sequence was implemented by directly modulating the dc current of the VCSEL, avoiding the use of any external AOM or optical shutter. The sequence generation, data acquisition, processing and corrections for servo loops are handled by a single Red Pitaya FPGA-board. To ensure proper clock operation and mitigate limitations caused by current-induced thermal transients in the laser, a real-time detection window tracking system was implemented. The clock frequency dependence to microwave power, laser power and laser frequency variations was significantly reduced with respect to Ramsey-CPT spectroscopy, up to a factor 27.5 for the microwave power. Over a 3-days measurement, the SABR-CPT microcell clock demonstrates a fractional frequency stability of 8×10^{-10} at 1 s and in the 10^{-12} range at 10^5 s. The stability at 1 day is comparable to the one obtained in Ref.²¹, in which an external AOM was used to produce the SABR sequence, and is among best results reported so far for microcell-based CPT clocks^{8,21,33}. These results might pave the way to the development of a new-generation of CPT-based CSACs, using Ramsey-based sequences, with reduced light-shifts, and improved long-term stability.

References

- 1. Kitching, J. Chip-scale atomic devices. Appl. Phys. Rev. 5, 031302 (2018).
- 2. Dicke, R. H. The effect of collisions upon the Doppler width of spectral lines. *Phys. Rev.* 89, 472–473 (1953).
- **3.** Alzetta, G., Gozzini, A., Moi, L. & Orriols, G. An experimental method for the observation of r.f. transitions and laser beat resonances in oriented Na vapour. *Il Nuovo Cimento B* **36**, 5–20 (1976).
- **4.** Zhu, M. & Cutler, L. S. Theoretical and experimental study of light shift in a CPT-based Rb vapor cell frequency standard. *32nd Annu. Precise Time Time Interval (PTTI) Meet.* 311–323 (2000).
- **5.** Shah, V. *et al.* Continuous light-shift correction in modulated coherent population trapping clocks. *Appl. Phys. Lett.* **89**, 151124 (2006).
- **6.** Zhang, Y., Yang, W., Zhang, S. & Zhao, J. Rubidium chip-scale atomic clock with improved long-term stability through light intensity optimization and compensation for laser frequency detuning. *J. Opt. Soc. Am. B* **33**, 1756–1763 (2016).
- **7.** Vaskovskaya, M. I. *et al.* Effect of the buffer gases on the light shift suppression possibility. *Opt. Exp.* **27**, 35856–35864 (2019).
- **8.** Yanagimachi, S., Harasaka, K., Suzuki, R., Suzuki, M. & Goka, S. Reducing frequency drift caused by light shift in coherent population trapping-based low-power atomic clocks. *Appl. Phys. Lett.* **116**, 104102 (2020).
- 9. Miletic, D. et al. AC Stark-shift in CPT-based Cs miniature atomic clocks. Appl. Phys. B 109, 89 (2012).

- **10.** Yudin, V. I. *et al.* General methods for suppressing the light shift in atomic clocks using power modulation. *Phys. Rev. Appl.* **14**, 024001 (2020).
- **11.** Abdel Hafiz, M. *et al.* Protocol for light-shift compensation in a continuous-wave microcell atomic clock. *Phys. Rev. Appl.* **14**, 034015 (2020).
- **12.** Basalaev, Y. M. *et al.* Dynamic continuous-wave spectroscopy of coherent population trapping at phase-jump modulation. *Phys. Rev. Appl.* **13**, 034060 (2020).
- **13.** Thomas, J. E. *et al.* Observation of Ramsey fringes using a stimulated, resonance Raman transition in a sodium atomic beam. *Phys. Rev. Lett.* **48**, 867–870 (1982).
- **14.** Zanon, T. *et al.* High contrast Ramsey fringes with coherent-population-trapping pulses in a double lambda atomic system. *Phys. Rev. Lett.* **94**, 193002 (2005).
- **15.** Boudot, R., Maurice, V., Gorecki, C. & de Clercq, E. Pulsed coherent population trapping spectroscopy in microfabricated Cs–Ne vapor cells. *J. Opt. Soc. Am. B* **35**, 1004–1010 (2018).
- **16.** Carlé, C. *et al.* Exploring the use of Ramsey-CPT spectroscopy for a microcell-based atomic clock. *IEEE Trans. Ultrason. Ferroelec. Freq. Contr.* **68**, 3249–3256 (2021).
- **17.** Abdel Hafiz, M. *et al.* Symmetric autobalanced Ramsey interrogation for high-performance coherent population- trapping vapor-cell atomic clock. *Appl. Phys. Lett.* **112**, 244102 (2018).
- **18.** Sanner, C., Huntemann, N., Lange, R., Tamm, C. & Peik, E. Autobalanced Ramsey spectroscopy. *Phys. Rev. Lett.* **120** (2018).
- **19.** Abdel Hafiz, M. *et al.* Light-shift mitigation in a microcell-based atomic clock with symmetric auto-balanced Ramsey spectroscopy. *Appl. Phys. Lett.* **120**, 064101 (2022).
- **20.** Carlé, C. *et al.* Reduction of helium permeation in microfabricated cells using alumino-silicate substrates and Al₂O₃ coatings. *J. Appl. Phys.* **133**, 214501 (2023).
- **21.** Carlé, C. *et al.* Pulsed-CPT Cs-Ne microcell atomic clock with frequency stability below 2×10^{-12} at 10^5 s. *Opt. Express* **31**, 8160–8169 (2023).
- 22. Ide, T., Goka, S. & Yano, Y. CPT pulse excitation method based on VCSEL current modulation for miniature atomic clocks. *Proc. Int. Freg. Control. Symp. Eur. Freg. Time Forum Jt. Meet.* 269–290 (2015).
- 23. Fukuoka, M., Goka, S., Kajita, M. & Yano, Y. Light shift of Ramsey-coherent population trapping resonance using drive current modulation. *Jpn. J. Appl. Phys.* 62, 122005 (2023).
- **24.** Fukuoka, M. & Goka, S. Simultaneous observation of semi-continuous and ramsey-coherent population trapping resonances using the ramsey pulse sequence with drive current modulation. *Jpn. J. Appl. Phys.* **63**, 012005 (2024).
- **25.** Rivera-Aguilar, C. M. *et al.* Operation of a Ramsey-CPT microcell atomic clock with driving current-based power modulation of a vertical-cavity surface-emitting laser. *Appl. Phys. Lett.* **124**, 114102 (2024).
- **26.** Kroemer, E. *et al.* Characterization of commercially available vertical-cavity surface-emitting lasers tuned on Cs D₁ line at 894.6 nm for miniature atomic clocks. *Appl. Opt.* **55**, 8839–8847 (2016).
- **27.** Hasegawa, M. *et al.* Microfabrication of cesium vapor cells with buffer gas for MEMS atomic clocks. *Sensors Actuators A* **167**, 594–601 (2011).
- **28.** Vicarini, R. *et al.* Demonstration of the mass-producible feature of a Cs vapor microcell technology for miniature atomic clocks. *Sens. Actuat. A: Phys.* **280**, 99 106 (2018).
- **29.** Hemmer, P. R., Shahriar, M. S., Natoli, V. D. & Ezekiel, S. Ac Stark shifts in a two-zone Raman interaction. *J. Opt. Soc. Am. B* **6**, 1519 (1989).
- **30.** Abdel Hafiz, M. et al. A high-performance Raman-Ramsey Cs vapor cell atomic clock. J. Appl. Phys. **121**, 104903 (2017).
- **31.** Breurec, J., Abdel Hafiz, M., Calosso, C. E., Lelièvre, O. & Boudot, R. Frequency shifts in a coherent population trapping Cs vapor cell atomic clock. *IEEE Trans. Ultrason. Ferroelec. Freq. Contr.* DOI: 10.1109/TUFFC.2025.3575002 (2025).
- 32. Martinez, G. D. et al. A chip-scale atomic beam clock. Nat. Commun. 14, 3501 (2023).
- **33.** Zhang, H. *et al.* ULPAC: A miniaturized ultra-low-power atomic clock. *IEEE Journ. Solid State Circuits* **54**, 3135–3148 (2019).

Acknowledgements

This work was supported by the Direction Générale de l'Armement (DGA) and by the Agence Nationale de la Recherche (ANR) in the frame of the ASTRID project named PULSACION (Grant ANR-19-ASTR-0013-01), LabeX FIRST-TF (Grant ANR 10-LABX-48-01), EquipX Oscillator-IMP (Grant ANR 11-EQPX-0033) and EIPHI Graduate school (Grant ANR-17-EURE-0002). The PhD thesis of C. Rivera is co-funded by the program FRANCE2030 QuanTEdu (Grant ANR-22-CMAS-0001) and Centre National d'Etudes Spatiales (CNES). This work was partly supported by the french RENATECH network and its FEMTO-ST technological facility (MIMENTO).

Author contributions statement

C-M.R-A. mounted the clock setup, developed the clock pilot software, programmed the FPGA, conducted experiments, prepared the figures for the manuscript, contributed to results analysis and to the manuscript writing. A.M. fabricated the Cs-Ne microfabricated vapor cell. C.C. participated to first experimental investigations. J.M.F supported C-M.R-A. for digital electronics. E.K. supported the results analysis. M. A-H. contributed to the SABR sequence design, data analysis and light shift studies. N.P. contributed to the design, fabrication and validation of the MEMS cell technology, and helped with the manuscript writing. R.B. proposed the investigation of Ramsey-based sequences in microcell CPT clocks, oversaw the project, contributed to the SABR sequence design, contributed to the results analysis, and wrote the first draft version of the manuscript. All authors reviewed the manuscript.

Competing interests

The authors declare no competing interests.

Ethics approval

This research is an original work of the authors and has not been previously published elsewhere.

Consent to participate

All authors have consented to participate in this research.

Data availability statement

The data of this study are available from the corresponding author upon reasonable request.